

OSCI-LIGHT: Oscillators based Synchronization for Visible Light Communication Systems

Valeria Loscri
Inria Lille, France
valeria.loscri@inria.fr

Rosane Ushirobira
Inria Lille, France
rosane.ushirobira@inria.fr

Antonio Costanzo
Université Gustave Eiffel, France
antonio.costanzo@univ-eiffel.fr

Denis Efimov
Inria Lille, France
denis.efimov@inria.fr

Abstract

Visible Light Communication paradigm has been expedited by the fast evolving and deployment of light emitting diodes (LED), and the possibility to simultaneously exploit the communication and illumination, enabling seamless connectivity based on the lighting infrastructure. Synchronization is a big deal in all the wireless communication systems and the key features of VLC paradigm make the synchronization techniques existing for RF not suitable for VLC.

A novel technique, OSCI-LIGHT based on Andronov-Hopf oscillators, is proposed in this work in order to realize an effective synchronization mechanism in a VLC system. In particular, phase alignment and robustness towards noise have been tested through both numerical simulation and experimental results and a comparison with widely employed synchronization techniques, based on Phase Locked Loop (PLL), has been provided. Experimental results show that our technique outperforms PLL techniques in terms of noise robustness, showing a proper steady state phase delay and a lower Synchronization Error Rate, even in presence of highly noisy environmental conditions.

Keywords

Visible Light Communication, Synchronization, Oscillators, Phase Locked Loop

1 Introduction

The research competition on 6G technologies has already started, even though the 5G technology is just being deployed worldwide. Visible Light Communication (VLC) is considered as one of the candidate technolo-

gies for 6G [1] [2], and it has attracted a tremendous amount of attention from both academia and industry.

VLC paradigm is based on the reuse of common lighting infrastructures based on Light Emitting Diodes (LED) [3]. The main purpose, indeed, is adding wireless communication data to those systems which are normally employed for brightening indoor environments, like lightening systems in buildings, or outdoor environments, like street lights and car lamps.

This paradigm has recently started to gain momentum in the research and industry community, for its efficiency in both terms of overall costs and energy consumption. In addition, since LED luminaries are present in almost each environment, high-speed data transmission is expected to be available everywhere. Furthermore, VLC systems aim to guarantee ubiquity requirements as requested by next generation wireless networks. Even if Visible Light architectures have been widely studied and developed, especially in last ten years, some important issues still limit their employment in real scenarios, and consequently, their full entrance in the market.

Noise and interference due to other light sources in the operative environment could often reach a critical level, preventing correct communication, especially in outdoor applications, where sunlight represents the main issue. In addition, VLC communication suffers in performing medium and long coverage operations, because of atmospheric absorption, shadowing, beam dispersion etc. The light source produced by LEDs is not coherent, real and unipolar. Signals are usually implemented using an intensity modulation and direct detection (IM/DD), and Non-linear clipping makes synchronization hard in these techniques. Most of signal processing techniques, typically used in Radio Frequencies (RF), cannot be transparently adapted for free space optics operations, required by VLC paradigm.

Synchronization could represent, in many practical applications, one of the major issues, especially in those modulations which require an accurate clock alignment between the transmitter and the receiver.

Pulse Position Modulation (PPM) and its variants,

like Inverse Pulse Position Modulation (IPPM) and Variable Pulse Position Modulation (VPPM) are widely used in VLC schemes because of their robustness to noise. However, since these modulations codify each symbol, using a specific position of the related time slot, a strict synchronization is required. Other types of modulation widely used in VLC for their performance, like Orthogonal Frequency Division Multiplexing (OFDM) and Carrierless Amplitude and Phase Modulation (CAP) need an accurate synchronization, too. In OFDM, indeed, it is necessary that the frequencies are accurately tracked to ensure that orthogonality is maintained, and as well as in PPM or in CAP, it is necessary that the sampling occurs at the correct time interval to ensure that the samples are synchronized and data errors are minimized.

An earlier discussion about timing and carrier recovery in optical systems started in late 70's, in the context of the novel communication based on optical fibers. The first discussion, tackling synchronization issues for optical systems, has been provided in [4], where the authors examine the effects of imperfect timing in non coherent direct-detection optical 2PPM. In [5] the authors investigated the performance of phase-locked loop (PLL) synchronized optical PPM communication with different index. However, since the employment of free space optics (FSO) for a real scenario has a relative recent history, related papers started to appear in the beginning of last decade. As a matter of fact, synchronization is still an important issue in the VLC systems and has an important impact on the system's performance. Based on these premises, in this work we investigated a new approach for achieving efficient and effective synchronization in a VLC system based on oscillators.

The main contributions can be summarized as follows:

- We propose OSCILIGHT, a synchronization method based on Andronov-Hopf oscillators
- We theoretically demonstrate the properties of our synchronization system in terms of phase alignment and synchronization time
- We prove the feasibility and validate the performance of our synchronization system, by implementing it in a real test-bed.

In particular, we integrate the approach in an experimental setup and compare the performance with widely used synchronization approaches based on Phased-Locked Loop (PLL) methods, proving the superiority of our approach.

The rest of the paper is organized as follows. In Section 2, we revise and discuss the main approaches in literature for synchronization purpose in VLC. In Section 3 we detail the specific architecture in this work and we explain the specific channel model and modulation technique considered. In Section 4, we give a detailed description of the problem from a mathematical point of view. The synchronization protocol is then presented in 5. In Section 6 we provide an analysis of

the performance of the synchronization system. Finally, we conclude the paper in Section 7.

2 Related Works

In this section we revise the most representative results achieved in terms of synchronization in optical wireless communication and VLC systems. As highlighted in [6], the time domain modulation approaches adopted in VLC, are extremely sensitive to time synchronization. Indeed, in [6] a mathematical model of the Bit Error Rate, in presence of clock jitter, has been presented and the effect of time synchronization for the IPPM has been evaluated. In [7] some more details on clock time shift and jitter in terms of BER performance are provided and the minimum requirements of the synchronization system are derived. In [8], polynomial fitting, threshold and under-sampling have been used to synchronize camera VLC signals, exploiting the rolling shutter effect of CMOS sensors. In [9], ad hoc frames are used for synchronizing under-sampled phase shift ON-OFF keying (UPSOOK) signals. Furthermore, the problem of synchronization of Carrierless Amplitude and Phase Modulation in VLC systems, has been discussed in [11].

Ad hoc frames are also used in [10], for identifying and synchronizing VLC signals in a multi-modulation scenario, based on the coexistence of PPM and Pulse Amplitude Modulation (PAM), with different indexes.

In [14], CMOS sensors are exploited by using a combination of Color Shift Keying (CSK), with a modified PPM modulation, in order to improve synchronization for the color detection.

In [15], a low cost time unit has been developed for synchronizing VLC system. It has been developed and tested in a low noise and low data rate application. A similar front-end has been used in [16], for recovering the carrier of optical signals based on ON-OFF keying.

A serious problem in most of the implementations mentioned above, is due to slow rate of convergence of synchronization algorithms and the use of long static pilot symbols sequences or preambles. In fact, a long pilot sequence is used from one side to reduce the synchronization error, but it significantly reduces system performance as well, when channel conditions would be favorable for a high data rate transmission. Moreover, it could be not suitable for real time operations, when channel conditions are not good, because of the need to employ even longer sequences to contrast noise effects.

Some papers deal with these issues in different ways. The problem of an adaptive Carrier Recovery in VLC signals has been studied in [17], where a Learning Approach based on multi-arm bandit has been exploited in highly noisy VLC scenarios.

A learning approach is also proposed in [18], where Golay sequences have been exploited for block synchronization and channel estimation in optical systems with IM/DD.

Other schemes make use of chaotic models for encrypting data and achieving an affordable synchroniza-

tion. Furthermore, these techniques also improve data security at the physical layer. A chaos synchronization scheme in the context of VLC, based on the inverse system approach with Lorenz oscillators, has been proposed in [19], while, a similar scheme, based on a chaotic Colpitts oscillator, has been developed and numerically validated in [20] in presence of Multipath Fading. A nonlinear system has been also exploited for synchronizing underwater vehicles through VLC in [22]. Their approach has been validated through simulations using 4PPM signals. The last published technique, using a similar approach for encrypting VLC data, is based on a Rossler chaotic system and it has been recently considered in [21], where a simple proportional integral derivative (PID) controller is used for improving synchronization. A novel synchronization algorithm, based on negative mirror image (NMI) algorithm and using an ad hoc training sequence, is proposed in [23] for OFDM, while, in the same scenario, a blind timing synchronization algorithm has been developed in [24]. In last years, some interesting studies have been focused on the possibility of using VLC for synchronizing operations in heterogeneous wireless sensor networks, where devices which exploit different technologies coexist and communicate each other. An implementation in a real scenario, for instance, has been already provided in [25], where VLC is used to feed, to synchronize time and to deliver the commands to the sensor nodes in an heterogeneous network for space applications, in the context of Ariane 5 program. A different approach, which also deals with synchronization in a heterogeneous architecture via Visible Light, is proposed in [26], where a De Bruijn sequence provides a rough estimation of time, using a minimum amount of information. The employment of VLC in mixed networks, as well as the entrance in the market of low cost, flexible and affordable VLC architectures, could raise, in next years, the interest of the scientific community to give a more focus on advanced and more performing synchronization techniques. These recent research results show the fervent interest on synchronization techniques in VLC and the urgency of robust synchronization mechanisms able to guarantee high efficiency in real-time applications.

3 System Model

In this Section, we detail the modules of the architecture considered for implementing the synchronization approach, we describe the channel model and the modulation techniques adopted in this work.

3.1 System Architecture

Our optical communication and signal processing, shown in Figure 1, is based on two Universal Software Radio Peripheral (USRP) 2922, a universal platform, provided by National Instruments, while low frequency daughter-boards, both provided by Ettus, have been added in the transmitting and receiving chain in order to allow modulation and demodulation in the range [0-30 MHz]. A bias tee and a single stage amplifier are used for allowing Led driving in the proper range. In

addition, an amplifying and conditioning network has been designed in order to allow the receiving signal to be correctly detected in the dynamic range of the receiving USRP. The first amplifier network allows the photodiode to be correctly polarized and the signal to be in the correct range for the second amplifying network, which performs the high gain trans-impedance amplification. An additive DC block capacitor mitigates the high DC component due to amplifiers, in order to avoid saturation of the USRP receiver. A 12V power supply feeds both the amplifiers. Uplink communication is performed using Arduino Uno and it is only used to exchange feedback messages, potentially allowing adaptive operations. In order to reduce hardware costs and improve system flexibility, most of signal processing operation (i.e. signal generation, filtering, modulation, demodulation, time recovering and data evaluation) are performed via software, using the commercial software Labview for the main communication and the Arduino IDE for feedback communication. Obviously, all synchronization operations have been implemented in software for all the described configurations.

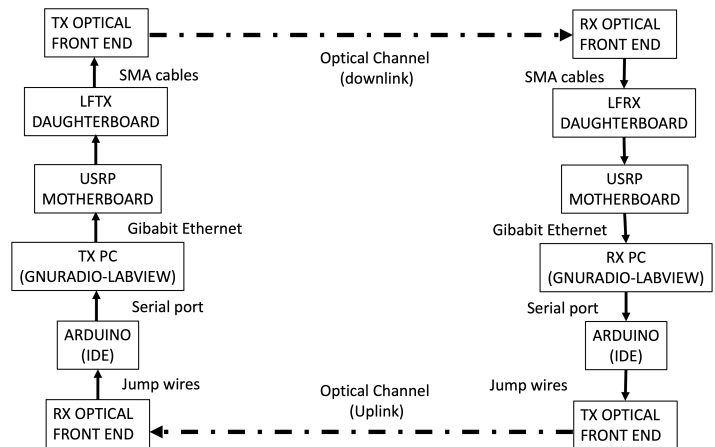


Figure 1. System Architecture

3.2 Channel Model

The ratio between the optical radiated power in the main direction $P_{T_{opt}}$, and the received optical power at a certain distance d can be modeled by considering the LED as a Lambertian source [3]. Indeed, assuming -3dB beam width of the LED equal to ϕ_{-3dB} , received power can be calculated as follows :

$$P_{R_{opt}} = P_{T_{opt}} \frac{(m+1)A}{2\pi d^2} \cos^m(\phi) T(\psi) g(\psi) \quad (1)$$

being:

- A the effective area of the photodiode;
- d the distance between transmitter and receiver;
- ϕ the angle of irradiance with respect to the axis normal to the transmitter surface;

- ψ the angle of incidence with respect to the axis normal to the receiver surface;
- $T(\psi)$ the gain of optical filter;
- $G(\psi)$ the receiver optical concentrator gain;
- m the order of the Lambertian Radiation

In particular, Lambertian order is calculated as follows

$$m = \frac{\ln 2}{\ln(\cos(\phi - 3dB))} \quad (2)$$

while the gain of the optical concentrator can be calculated, starting by its refraction index η and by the field of view of the receiver ψ_0 , as follows:

$$G(\psi) = \frac{\eta^2}{\sin^2(\psi_0)} \quad (3)$$

3.3 Modulation technique

The modulation schemes we consider in this work are 2-, 4-, 8-, 16- Pulse Position Modulation, in order to achieve high reliability at the expense of transmission rate, especially when higher modulation indexes are employed. PPM signaling is represented by the following relationship

$$s_d(t) = x(t - \Delta_\ell T_p) \quad (4)$$

where x is the transmitted signal, Δ_ℓ describes the delay ranging from 0 to $M - 1$ as multiple integer of T_p elementary delay equating, at least, the pulse length in order to grant orthogonality among PPM symbols. In our implementation, we considered that each PPM symbol presents an intensity equating P^{\max} so the energy among a PPM symbol is $E_{PPM} = P^{\max}/MT_p$.

4 Problem statement

In this work, we rely on the property of periodic signal that can be related with an oscillator output *i.e.*, a dynamical system whose state performs periodical movements. In particular, we focus on Andronov-Hopf oscillator, where among the several periodic trajectories, each is locally attracting/repulsing and forms a limit cycle.

The Andronov-Hop can be described as:

$$\dot{x}_i(t) = Ax_i(t) + \omega k(1 - |x_i(t)|^2)x_i(t) + \delta_i(t), t \geq 0, \quad (5)$$

$$A = \begin{pmatrix} 0 & \omega \\ -\omega & 0 \end{pmatrix},$$

for all $i \in N^*$ (the set of nonzero positive integers), where $x_i(t) = (x_{i1}(t) \ x_{i2}(t))^T \in \mathbb{R}^2$ is the state of the i th oscillator; $\delta_i(t) \in \mathbb{R}^2$ is an external (bounded) input; $\omega > 0$ is the oscillation frequency; $k > 0$ is the attraction gain and $|\cdot|$ is the Euclidean norm on \mathbb{R}^2 . For $\delta_i \equiv 0$, for all $i \in N^*$, this oscillator has its limit cycle on the unit circle with $|x_i| \equiv 1$, where all solutions are harmonic signals of frequency ω , as demonstrated in the Appendix. An unstable equilibrium is identified in the origin. For any bounded input δ_i , the trajectories of (5) stay bounded approaching a vicinity of the limit

cycle (or the origin), whose size is proportional to the amplitude of the input.

The oscillators in (5) can then model both the transmitter and the receiver with $i = 1$ and $i = 2$, respectively, with trajectories on the limit cycle having different initial conditions and $\delta_i \equiv 0$. Let

$$y_i(t) = h(x_i(t)), t \geq 0,$$

be the pulse generated by the oscillators for a suitably defined function h . Then the signal y_1 is sent by the transmitter, corrupted by a bounded noise $v(t) \in \mathbb{R}$ signal, and recovered by the receiver is

$$y(t) = y_1(t) + v(t).$$

An example of such an output map is

$$h(\xi) = \begin{cases} \mathbf{a} & \text{if } \arcsin(\xi_1) \geq \mathbf{b} \\ 0 & \text{if } \arcsin(\xi_1) < \mathbf{b} \end{cases}, \xi = (\xi_1 \ \xi_2)^T \in \mathbb{R}^2, \quad (6)$$

where $\mathbf{a} > 0$ and $\mathbf{b} \in (-\frac{\pi}{2}, \frac{\pi}{2})$ are parameters regulating the amplitude and the pulse width, respectively, or

$$h(\xi) = a(b - \tanh(\kappa(1 + \xi_1))), \quad (7)$$

where $a, b > 0$ determine the amplitude and $\kappa > 0$ parameterizes the pulse width.

By guaranteeing that $y_2(t) \rightarrow y_1(t)$ using the measurements of $y(t)$, we achieve the objective of the synchronization protocol.

Such an issue can be classified as the *phase synchronization* between oscillators (the phase determines the position of the trajectories $x_i(t)$ on the limit cycle). If we introduce the synchronization error $e = x_1 - x_2 = (e_1 \ e_2)^T \in \mathbb{R}^2$, then the posed problem can be formulated as a robust (concerning the noise v) stabilization of e .

5 Synchronization protocols

In this work, we consider a simple scheme of synchronization, based on the injection of a direct synchronization error in the receivers as follows:

$$\delta_2(t) = L(y(t) - y_2(t)) = L(y_1(t) - y_2(t) + v(t)), \quad (8)$$

where $L \in \mathbb{R}^2$ is the coupling gain.

In literature is demonstrated that with a small noise measured, it is possible to apply the pulse synchronization theory [13]. It is mainly based on a phase dynamics analysis with the output as (6). By considering the phase response curve (PRC) approach, it is possible to analyze the pulse response, since the oscillator phase dynamics is one-dimensional, independently of the dimension of the state-space vector.

The synchronization problem becomes complicated if the measurement noise is significant and if the measured signal y has a shape severely deviated from a pulse. In such a case, a continuous output function as in (7) can be used.

Hence, we have the following result for (5) (denote by I_n the identity matrix of dimension $n \times n$ and by $\lambda_{\min}(P)$ the minimum eigenvalue of a real symmetric

matrix $P \in \mathbb{R}^{n \times n}$):

THEOREM 1. Consider two oscillators (5) with $\delta_1 \equiv 0$ and δ_2 given in (8) where the output (7) is used. Assume $|x_i(0)| = 1$ for $i = 1, 2$. Suppose there exists

$$0 < P = P^\top \in \mathbb{R}^{2 \times 2},$$

$$L \in \mathbb{R}^2, \alpha > 0, \rho > 0 \text{ and } \gamma > 0$$

such that

$$(A - \beta LC)^\top P + P(A - \beta LC) + \varrho C^\top C \leq -2\alpha P,$$

$$-PL = C^\top = [1 \ 0]^\top, \quad P \leq \gamma I_2,$$

$$\varrho = 2 \left(\frac{2\gamma}{\alpha} + \frac{\rho}{\omega k} \right) |L|^2 a^2 \kappa^2,$$

where

$$e_1 \left(\tanh(\kappa(1 + x_{11} - e_1)) - \tanh(\kappa(1 + x_{11})) - \frac{\beta}{a} e_1 \right) \leq 0 \quad (9)$$

for any $x_{11} \in [-1, 1]$, any $|e_1| \leq 2.15$ and some $\beta \in \mathbb{R}$. If the measurement noise admits a known upper bound $\bar{v} > 0$ (so $|v(t)| \leq \bar{v}$ for all $t \geq 0$) and

$$\frac{\sigma}{\omega^2 k^2} (4a^2 + \bar{v}^2) \leq \frac{1}{16},$$

then the synchronization error e stays bounded and

$$\lim_{t \rightarrow +\infty} |e(t)| \leq \sqrt{\frac{\frac{2}{\lambda_{\min}(P)} \left(3\frac{\gamma}{\alpha} + \frac{\rho}{\omega k} \right)}{\alpha \min \left\{ 1, \frac{\rho \omega k}{2\gamma \omega k + \alpha \rho} \right\}}} |L| \bar{v}.$$

PROOF. Since $|x_1(0)| = 1$ and $\delta_1 \equiv 0$, then $|x_1(t)| = 1$ for all $t \geq 0$, due to Lemma 1 (Appendix). Next, the proof is divided into three steps: first, the behavior of the driven system (5) with $i = 2$ is evaluated, and the boundedness of x_2 is shown. Second, the stability of the synchronization error e is investigated. Third, the composed dynamics is analyzed, showing that the systems are synchronized on the unit cycle with the error proportional to the amplitude of the measurement noise.

1) Following the proof of Lemma 1, consider the Lyapunov function

$$W(x_2) = \frac{1}{2} (1 - |x_2|^2)^2$$

for the driven system, whose derivative for the dynamics of (5) with $i = 2$ admits an estimate:

$$\dot{W} \leq -\omega k (1 - |x_2|^2)^2 |x_2|^2 + \frac{1}{\omega k} \delta_2^\top \delta_2.$$

Note that

$$\begin{aligned} \delta_2^\top \delta_2 &= (y_1 + v - y_2)^\top L^\top L (y_1 + v - y_2) \\ &\leq 2(y_1 - y_2)^\top L^\top L (y_1 - y_2) + 2v^\top L^\top L v \\ &= 2a^2 (\tanh(\kappa(1 + x_{21})) - \tanh(\kappa(1 + x_{11})))^\top L^\top L \\ &\quad \times L (\tanh(\kappa(1 + x_{21})) - \tanh(\kappa(1 + x_{11}))) \\ &\quad + 2v^\top L^\top L v. \end{aligned}$$

Since

$$\begin{aligned} (\tanh(\kappa(1 + x_{21})) - \tanh(\kappa(1 + x_{11})))^2 &\leq \kappa^2 (x_{21} - x_{11})^2 \\ &\leq \kappa^2 e_1^\top e_1, \end{aligned}$$

for all $x_{11}, x_{21} \in \mathbb{R}$ and $e_1 = x_{11} - x_{21}$, finally we obtain:

$$\dot{W} \leq -\omega k (1 - |x_2|^2)^2 |x_2|^2 + 2|L|^2 \frac{a^2 \kappa^2 e_1^\top e_1 + v^\top v}{\omega k}. \quad (10)$$

From another side,

$$\begin{aligned} \delta_2^\top \delta_2 &\leq 2(y_1 - y_2)^\top L^\top L (y_1 - y_2) + 2v^\top L^\top L v \\ &\leq 2|L|^2 \left((y_1 - y_2)^\top (y_1 - y_2) + v^\top v \right) \\ &\leq 2|L|^2 (4a^2 + \bar{v}^2), \end{aligned}$$

hence,

$$\dot{W} \leq -\omega k (1 - |x_2|^2)^2 |x_2|^2 + \frac{2|L|^2}{\omega k} (4a^2 + \bar{v}^2), \quad (11)$$

and it is straightforward to check that if

$$\frac{2|L|^2}{\omega^2 k^2} (4a^2 + \bar{v}^2) \leq \frac{1}{8},$$

then the set

$$\mathcal{X} = \{x_2 \in \mathbb{R}^2 : \sqrt{0.5} \leq |x_2| \leq 1.144\}$$

is forward invariant for the driven system. Therefore, $x_2(t) \in \mathcal{X}$ for all $t \geq 0$ since $x_2(0) \in \mathcal{X}$, which also leads to the constraint:

$$|e(t)| \leq 2.144, \quad \forall t \geq 0.$$

2) The dynamics of the estimation error e can be written as

$$\begin{aligned} \dot{e} &= Ae - \omega k (1 - |x_2|^2) x_2 - L(y_1 + v - y_2) \\ &= (A - \beta LC)e - \omega k (1 - |x_2|^2) x_2 \\ &\quad - L(y_1 - y_2 - \beta Ce) - Lv \end{aligned}$$

with $\beta \in \mathbb{R}$ given in the theorem's statement. Consider a Lyapunov function for the synchronization error dynamics:

$$V(e) = e^\top P e,$$

where the matrix P is defined in the formulation of the theorem. Its derivative takes the form (recall that $-e^\top PL(y_1 - y_2 - \beta Ce) \leq 0$ by the imposed condition (9)):

$$\begin{aligned}
\dot{V} &\leq -2\alpha e^\top P e - \rho e^\top C^\top C e \\
&\quad - 2e^\top P (\omega k(1 - |x_2|^2)x_2 + L(y_1 - y_2 - \beta C e) + L v) \\
&\leq -2\alpha e^\top P e - \rho e^\top C^\top C e - 2e^\top P (\omega k(1 - |x_2|^2)x_2 + L v) \\
&\quad \leq -\alpha e^\top P e - \rho e^\top C^\top C e \\
&\quad + \frac{2}{\alpha} \left(\omega^2 k^2 (1 - |x_2|^2)^2 x_2^\top P x_2 + v^\top L^\top P L v \right) \\
&\quad \leq -\alpha e^\top P e - \rho e^\top C^\top C e \\
&\quad + \frac{2\gamma}{\alpha} \left(\omega^2 k^2 (1 - |x_2|^2)^2 |x_2|^2 + |L|^2 v^\top v \right). \quad (12)
\end{aligned}$$

3) Finally, for given $\rho > 0$, introduce a Lyapunov function

$$U(e, x_2) = V(e) + \left(\frac{2\gamma}{\alpha} \omega k + \rho \right) W(x_2),$$

then according to the derived estimates (10) and (12) we obtain (recall that $\sqrt{0.5} \leq |x_2|$):

$$\begin{aligned}
\dot{U} &\leq -\alpha e^\top P e - \rho \omega k (1 - |x_2|^2)^2 |x_2|^2 \\
&\quad + 2|L|^2 \left(3\frac{\gamma}{\alpha} + \frac{\rho}{\omega k} \right) v^\top v \\
&\leq -\alpha e^\top P e - 0.5\rho \omega k (1 - |x_2|^2)^2 + 2|L|^2 \left(3\frac{\gamma}{\alpha} + \frac{\rho}{\omega k} \right) v^\top v \\
&\leq -\alpha \min \left\{ 1, \frac{\rho \omega k}{2\gamma \omega k + \alpha \rho} \right\} U + 2|L|^2 \left(3\frac{\gamma}{\alpha} + \frac{\rho}{\omega k} \right) \bar{v}^2,
\end{aligned}$$

which implies the result. \square

If (9) is verified for smaller values of e_1 , then the obtained result holds locally in the synchronization error. The introduced in this theorem linear matrix inequalities can be simplified at the price of a less precision estimate for the asymptotic behavior of the synchronization error:

COROLLARY 1. *Consider two oscillators (5) with $\delta_1 \equiv 0$ and δ_2 given in (8) where the output (7) is used. Assume $|x_i(0)| = 1$ for $i = 1, 2$. Suppose there exist*

$$0 < P = P^\top \in \mathbb{R}^{2 \times 2},$$

$$L \in \mathbb{R}^2, \alpha > 0, \rho > 0 \text{ and } \gamma > 0$$

such that

$$\begin{aligned}
(A - \beta LC)^\top P + P(A - \beta LC) &\leq -2\alpha P, \\
-PL = C^\top &= [1 \ 0]^\top, P \leq \gamma I_2,
\end{aligned}$$

with (9) for any $x_{11} \in [-1, 1]$, any $|e_1| \leq 2.15$ and some $\beta \in \mathbb{R}$. Assume that the measurement noise admits a known upper bound $\bar{v} > 0$ (so $|v(t)| \leq \bar{v}$ for all $t \geq 0$), and

$$\frac{\sigma}{\omega^2 k^2} (4a^2 + \bar{v}^2) \leq \frac{1}{16}.$$

Then the synchronization error e stays bounded and

$$\lim_{t \rightarrow +\infty} |e(t)| \leq \sqrt{\frac{2}{\lambda_{\min}(P)} \left(3\frac{\gamma}{\alpha} + \frac{\rho}{\omega k} \right)} |L| (\bar{v} + 2a).$$

$$\sqrt{\alpha \min \left\{ 1, \frac{\rho \omega k}{2\gamma \omega k + \alpha \rho} \right\}}$$

PROOF. The proof follows the line of the main result, but instead of using (10) we will apply (11), and since the matrix inequalities have been modified for the derivative of Lyapunov function V the following inequality can be obtained:

$$\dot{V} \leq -\alpha e^\top P e + \frac{2\gamma}{\alpha} (\omega^2 k^2 (1 - |x_2|^2)^2 |x_2|^2 + |L|^2 \bar{v}^2). \quad (13)$$

For given $\rho > 0$, applying the derived estimates (11) and (13) to the derivative of the Lyapunov function U we have:

$$\begin{aligned}
\dot{U} &\leq -\alpha e^\top P e - \rho \omega k (1 - |x_2|^2)^2 |x_2|^2 \\
&\quad + 2|L|^2 \left(\left(3\frac{\gamma}{\alpha} + \frac{\rho}{\omega k} \right) \bar{v}^2 + 4 \left(\frac{2\gamma}{\alpha} + \frac{\rho}{\omega k} \right) a^2 \right) \\
&\leq -\alpha \min \left\{ 1, \frac{\rho \omega k}{2\gamma \omega k + \alpha \rho} \right\} U \\
&\quad + 2|L|^2 \left(\left(3\frac{\gamma}{\alpha} + \frac{\rho}{\omega k} \right) (\bar{v}^2 + 4a^2) \right),
\end{aligned}$$

which implies the result. \square

The derived estimates on the asymptotic behavior of the synchronization error are rather conservative (which is a frequent issue in the analysis of nonlinear systems). However, the actual precision of the synchronization scheme is much better, as we are going to demonstrate through its application.

6 Performance Evaluation

In this section we demonstrate the feasibility of the synchronization technique explained in the previous section, by integrating it in the setup described in section 3. We compare the proposed synchronization method with PLL and modified PLL methods.

6.1 Time Domain

Using the setup described above, we evaluated the convergence time, namely the time, starting from the first received sample of the synchronization frame, in which the phase of the output signal is correctly locked to the one of the received sequence. Two different PLL schemes, typically considered by the literature, have been implemented and compared to our technique. In the first implementation, the PLL stage is simply composed of an oscillator, which generates a periodic signal, and a phase detector, which compares the phase of that signal with the phase of the input periodic signal, adjusting the oscillator to keep the phases matched [39]. The second implementation, a Multiple Voltage

Control Oscillator, including an optimum Time Varying Filtering stage has been considered [40]. In Fig. 2, 3, 4 and 5, it is shown the time domain behavior of input sequence and the output of the synchronizing block for 2PPM, 4PPM, 8PPM and 16PPM. We repeated the same evaluation, considering the same environmental scenario (SNR=10dB) and the same system parameters (pulse time $\tau = 50ms$ and sample time $t_s = 500ns$) for our technique and both PLL configurations. We considered an observation interval composed of the first 10 Symbol times of the synchronization frame.

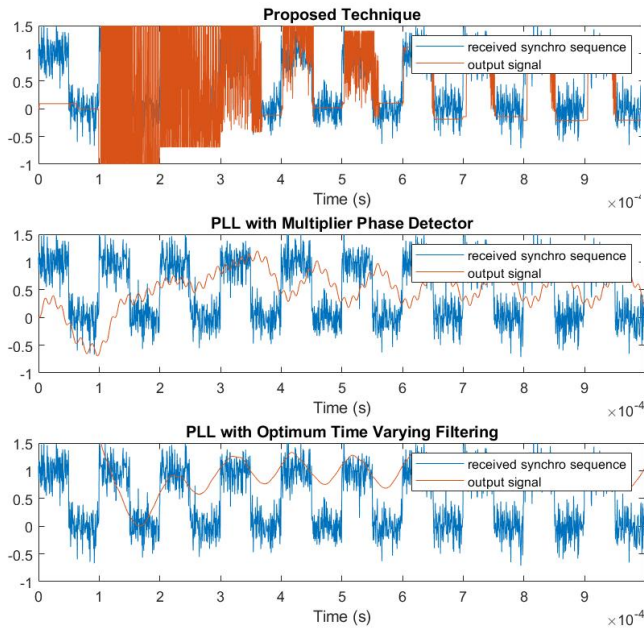


Figure 2. Starting Symbols of Synchronization Sequence for 2PPM Modulation Scheme

We notice how, for 2PPM and 4PPM synchronization frames, modified PPL scheme converges some symbols faster than our technique and the basic PPL scheme. Anyway, the difference is not so relevant in practical applications, since a frame of a certain duration (at least ten symbols) is always needed in order to avoid misunderstanding between starting frame symbols, data and eventually end sequences. In this case, since the difference is few symbol times, convergence is reached without need of additional time in all three configurations. We also notice how our technique outperform basic PLL in terms of noise tolerance and both techniques in terms of quality of the pulse shape, which appears quite distorted in the other techniques. This aspect becomes more evident when the distance between pulses increases, namely for higher modulation indexes. In addition, for 8PPM and 16PPM, convergence times are similar for all the configurations. Another important aspect is the steady state phase error, which is

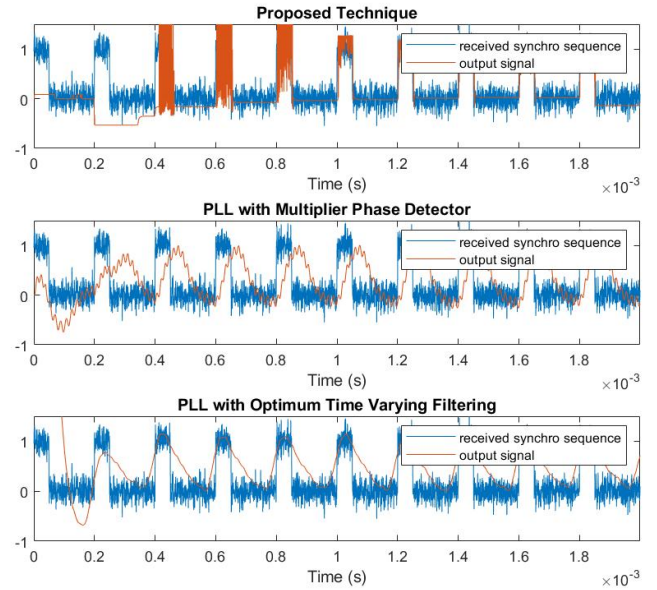


Figure 3. Starting Symbols of Synchronization Sequence for 4PPM Modulation Scheme

a permanent nonalignment between the input and the output signal once the phase has been locked, reducing the robustness of the synchronization and data recovering, especially if other phenomena, like clock shifts and phase noise occur during data communication. In order to evaluate, in a qualitative way, phase shift between input and output data, we show the behavior of synchronization block, for all the configurations, once the signal has correctly converged. We chose an observation time in the range between 20 and 30 time symbols after the first transmission.

In this case, our technique overcomes the other two techniques for all the modulation schemes, showing a very precise phase alignment between the input and the output of the synchronizing block.

6.2 Evaluation of Synchronization Error Probability

In order to quantitatively evaluate the performance of the proposed technique and provide a comparison with existing techniques based on PLL, we have performed a suite of targeted tests using both numerically generated signals and tested on a real VLC architecture, employing optical signals based on PPM with different indexes. In particular, we tested the effectiveness of our technique, employing synchronization frames based on 2, 4, 8 and 16 PPM. For simplicity, we considered in our tests a frame composed by a continuous transmission of the first symbol of the corresponding PPM modulation, in order to maintain the periodicity of the overall synchronization signal. We further estimated the Synchronization Error Probability, namely the percent-

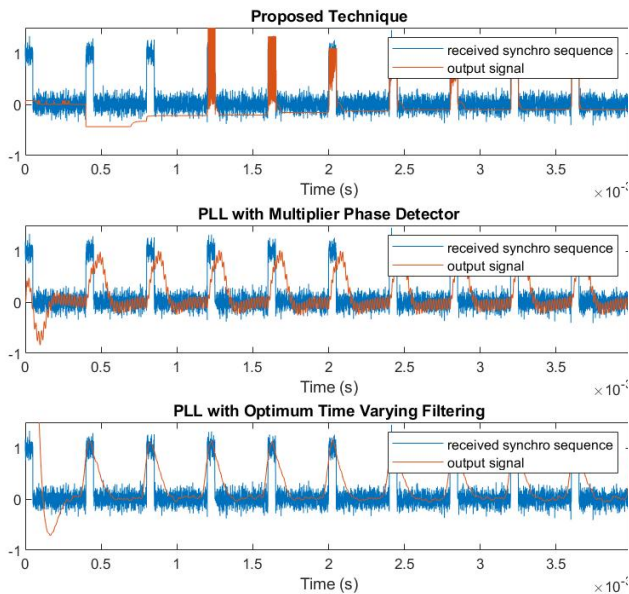


Figure 4. Starting Symbols of Synchronization Sequence for 8PPM Modulation Scheme

age of synchronization frames which are not correctly decoded by the receiver, because of nonalignment between the frame and the output signal or because of the high level of environmental noise. In particular, being τ the duration of each pulse, an error occurs when the signal in output to the receiver is delayed by the transmitted signal by a quantity greater than $\tau/2$. In this case, the position of all synchronization pulses can not be correctly received, and consequently, all the following user data are corrupted. Since we use PPM waveforms for codifying both synchronization sequence and user data, the estimation of Synchronization Error Probability is the same of the one which is employed for estimating BER, in PPM systems [36]. An extended suite of experimental tests has been provided, and a limited amount of data (equal to 1Msamples) has been collected for each test. However, in order to measure with high precision synchronization error, a very long observation should be set. For that reason, we estimate the BER using a semi-analytic technique, starting by measured received signals, instead of directly counting the error occurrences. The first step is the estimation of Signal to Noise Ratio (SNR), which is defined as the power of a signal of interest divided by the power of the noise affecting the system. In our case, we consider two main contributions which characterize received signal:

- The power associated to the signal of interest, S , is the power of PPM modulated signal received by the optical front-end, which allows the reconstruction of useful information.
- The power associated to the overall noise, N is con-

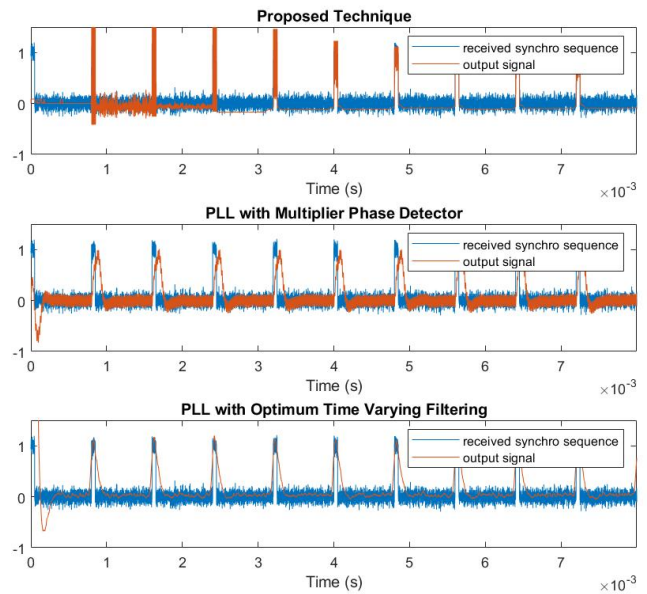


Figure 5. Starting Symbols of Synchronization Sequence for 16PPM Modulation Scheme

stituted by the shot noise (generated by the LED itself) and the thermal noise (generated by the amplifiers and the other components in the receiver) [8].

So, we can express SNR as:

$$SNR = \frac{S}{N} \quad (14)$$

For having an immediate synchronization and a comfortable analysis, in all the modulation schemes we used, we transmitted repeatedly the first symbol of the related alphabet. In particular, when 2PPM modulation is tested, a repetition of the symbol 0 is transmitted; in the same way, for the 4PPM the symbol 00, for 8 PPM the symbol 000 and for the 16PPM the symbol 0000 are transmitted. In this case, the useful signal is composed by a train of peaks, each peak delayed of a quantity T , equal to the symbol time. Being M the order of modulation and τ the duration of each pulse, symbol time can be expressed as:

$$T = M\tau \quad (15)$$

In order to obtain an estimation of the power associated to the useful signal in the whole transmitting time, we integrate the received $x(t)$ signal in the interval where the signaling pulse is supposed to be, and we consider an average between the power associated to all the received pulses. Being P the total number of transmitted symbols (and transmitted pulses), and p the index of each symbol, we estimate the power associated to the signal as:

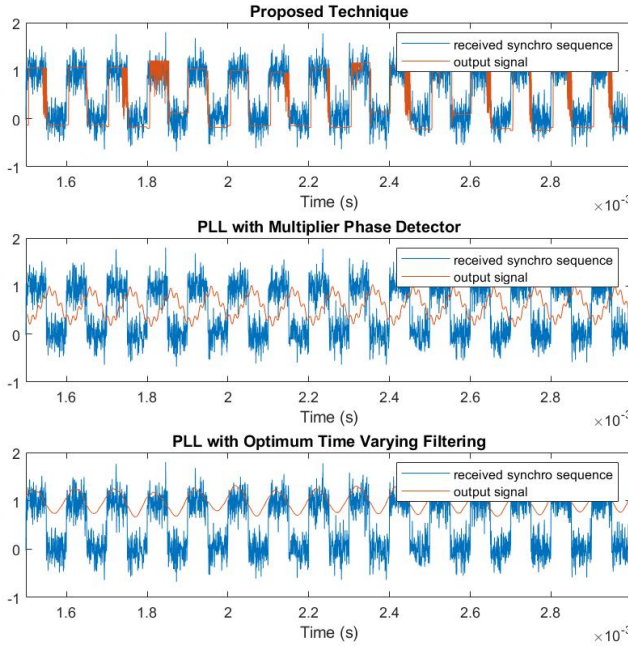


Figure 6. Ending Symbols of Synchronization Sequence for 2PPM Modulation Scheme

$$S = \frac{\sum_{p=0}^{P-1} \frac{1}{\tau} \int_{pT}^{pT+\tau} |x(t)|^2 dt}{P} \quad (16)$$

All the power associated to the received signal, which falls outside one of the time slots $[pT, pT + \tau]$, $\tau \in [0, P - 1]$, contributes to increase the term N . The estimation of the average power associated to noise and interference, becomes:

$$N = \frac{\sum_{p=0}^{P-1} \frac{1}{\tau} \int_{pT+\tau}^{(p+1)T} |x(t)|^2 dt}{P} \quad (17)$$

Since both thermal and shot noise, compounding the term N , follow a Gaussian behavior [3], the analytic description of BER can be analytically estimated [38]. As explained before, this error is equal to Synchronization Probability Error P_e of the known sequence received using the same modulation and the same system parameters. Since multiple AWGN components (i.e. shot noise, thermal noise) can be observed, we can consider total noise variance as the summation of individual noise variances due to properties of the Gaussian distribution [38]. According to this assumption, we can process the estimation of the effects of noise on Synchronization Error in the same way if we treat a Gaussian noise. The overall Synchronization Error is calculated, starting by SNR, as follows:

$$P_e = \frac{1}{2} \operatorname{erfc}\left(\frac{1}{\sqrt{2}} \sqrt{\operatorname{SNR} \frac{M}{2} \log_2 M}\right) \quad (18)$$

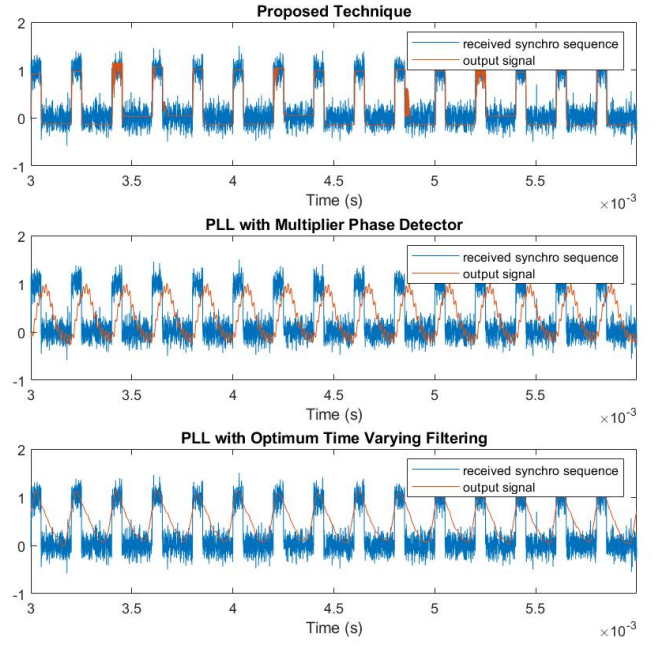


Figure 7. Ending Symbols of Synchronization Sequence for 4PPM Modulation Scheme

being erfc the operator corresponding to the Complementary Error Function, namely:

$$\operatorname{erfc}(x) = \int_0^x e^{-t^2} dt \quad (19)$$

Even if this technique represents an approximation of the exact Synchronization Error Probability, it is really useful for having a fast estimation, suitable for real time operations. Indeed, the quantity of data needed for obtaining P_e in this way is much lower than the one necessary for a direct counting of incorrect symbols. A comparison between the three techniques, and a comparison between simulated data, obtained by properly exploiting the channel model and measured data, is proposed in Fig. 10 and Fig. 11, where steady state phase delay and Estimated Synchronization Error Probability are shown for a 16PPM modulation, considering a pulse duration of 50 microseconds and a sample rate of 500 nanoseconds. Different environmental conditions have been taken into consideration in order to evaluate the robustness to noise of our technique.

The overall behavior of experimental data mainly follows the numerical model. Small bias effects, having no practical relevance, are due to some additive errors in the real scenario, due to imperfections and non linearity in optical components, amplifiers etc. In both cases, our technique outperforms PLL techniques in terms of noise robustness, showing a proper phase delay and a lower Synchronization Error Rate for all the value of

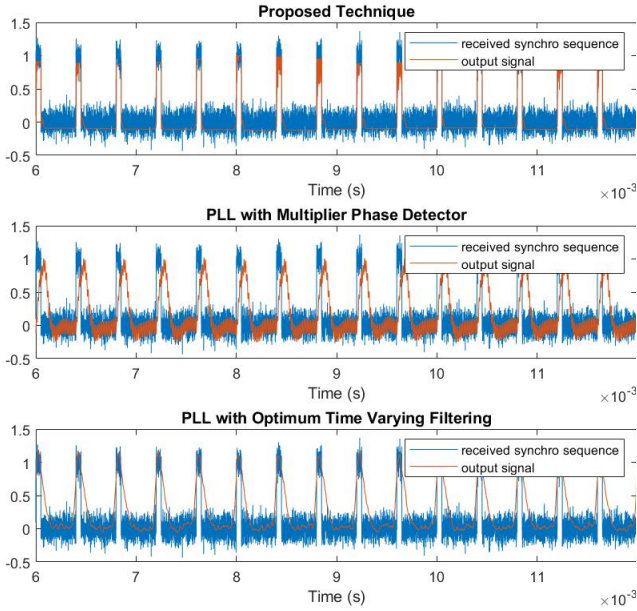


Figure 8. Ending Symbols of Synchronization Sequence for 8PPM Modulation Scheme

input SNR. Similar results have been obtained for the other modulation schemes. Since all the parameters, in all the three techniques, have been optimized for a pulse duration equal to 100 microseconds, a further analysis has been performed varying this value, and considering a strong noise component, which causes an input signal to noise ratio equal to 5 dB. Estimated Synchronization Probability is shown in Fig 12, where all the four PPM modulations have been considered for each one of the synchronization techniques.

In this last figure, we notice how for higher values of modulation index our system outperforms the other techniques, showing a larger bandwidth behavior. However, when the modulation index decreases, bandwidth limitation due to the poor sample rate of the considered hardware, degrade the signal for all the three techniques, preventing the correct calculation of output signal in our technique, since too few sample per pulse are provided in the receiving signal. In any case, our synchronization approach outperforms the other techniques, showing a more robust behavior also in high noise conditions.

7 Conclusions

The problem of signal synchronization in Visible Light Communication has been faced in this work. In particular, a novel technique, OSCI-LIGHT based on the exploitation of Andronov-Hopf oscillators has been proposed and analytically described. An optical Software Defined Platform, based on USRP, Arduino and low cost optical transceivers, has been developed and

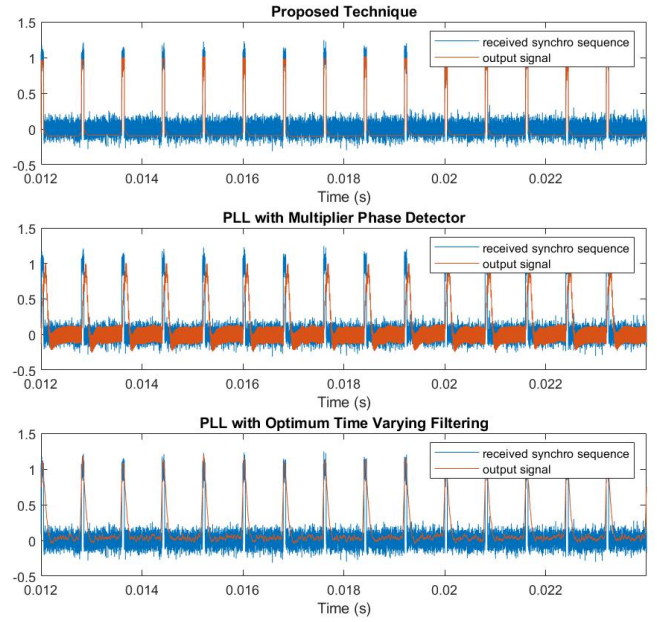


Figure 9. Ending Symbols of Synchronization Sequence for 16PPM Modulation Scheme

exploited in order to test the effectiveness of our approach. A comparison between our technique, a single stage and a multiple stage PLL has been shown. We considered, in our experimental campaign, Pulse Position Modulation with different indexes as transmitting signal and different noise conditions, in order to test the robustness of the approach also in difficult environmental conditions. Experimental results show a proper convergence of synchronization technique, comparable to the one performed by PLL techniques, but an improved robustness to noise and better performance in terms of steady state phase error and synchronization error probability.

Appendix

For $\delta_i \equiv 0$, the system (5) has two compact invariant sets: the origin $x_i = 0$ and the unit circle $|x_i| = 1$. It is easy to check that the origin is locally exponentially unstable, while on the unit circle the system equations are reduced to linear ones:

$$\dot{x}_i(t) = Ax_i(t),$$

whose solutions are harmonic with the frequency ω . Define the total invariant set by

$$\mathcal{W} = \{x_i \in \mathbb{R}^2 : \{0\} \cup |x_i| = 1\},$$

which is decomposable in this case.

For more details about definition and notions, such as input-to-state stability and invariant sets, please refer to [12].

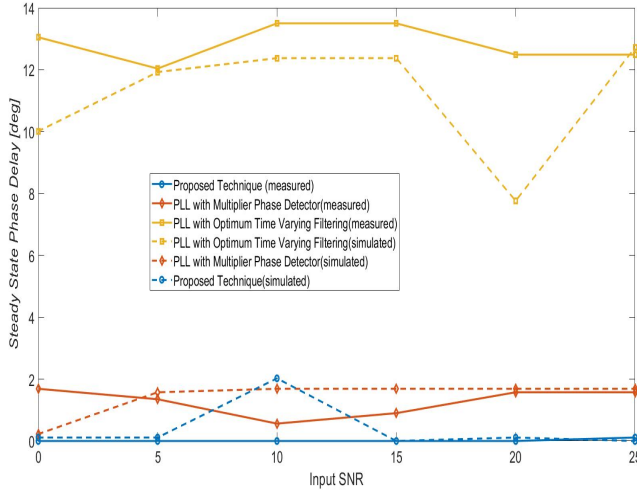


Figure 10. Steady State Error Phase: comparison between simulated and experimental results

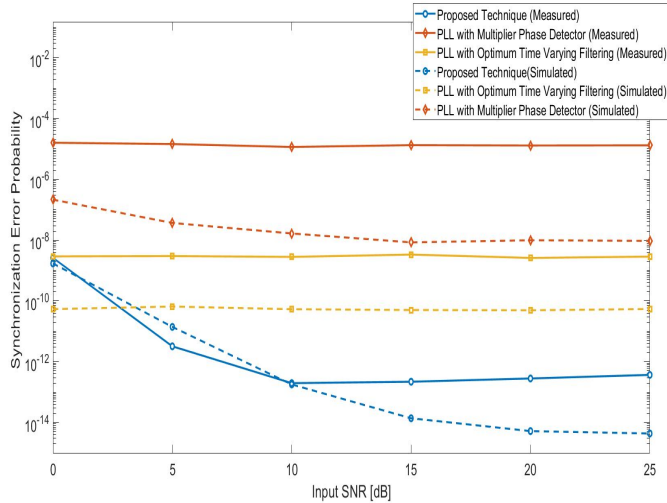


Figure 11. Synchronization Error Probability: comparison between simulated and experimental results

LEMMA 1. The system (5) is input-to-state stable with respect to the set \mathcal{W} and the input δ_i .

PROOF. Consider a Lyapunov function candidate:

$$W(x_i) = \frac{1}{2}(1 - |x_i|^2)^2,$$

whose derivative for the system takes the form:

$$\begin{aligned} \dot{W} &= -2(1 - |x_i|^2)x_i^\top \dot{x}_i \\ &= -2\omega k(1 - |x_i|^2)^2|x_i|^2 - 2(1 - |x_i|^2)x_i^\top \delta_i \\ &\leq -\omega k(1 - |x_i|^2)^2|x_i|^2 + \frac{1}{\omega k}\delta_i^\top \delta_i. \end{aligned}$$

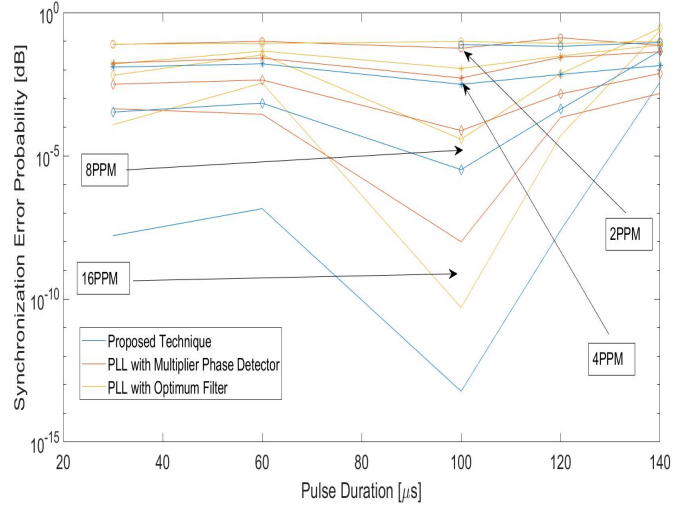


Figure 12. Synchronization Error Probability: Comparison between different modulation indexes, varying pulse time of PPM communication, in strong noise conditions

Clearly, there is a function $\psi \in \mathcal{K}_\infty$ (a continuous, zero at zero, strictly increasing and unbounded function $\mathbb{R}_+ \rightarrow \mathbb{R}_+$) such that for all $x_i \in \mathbb{R}^2$:

$$(1 - |x_i|^2)^2|x_i|^2 \geq \psi(|x_i|_{\mathcal{W}}),$$

where $|x_i|_{\mathcal{W}} = \inf_{z \in \mathcal{W}} |z - x_i|$ is the distance to the set \mathcal{W} , then

$$\dot{W} \leq -\omega k \psi(|x_i|_{\mathcal{W}}) + \frac{1}{\omega k} \delta_i^\top \delta_i,$$

which is equivalent to input-to-state stability property with respect to the set \mathcal{W} and the input δ_i . \square

The proven stability property also implies that if $\delta_i = 0$, then almost all trajectories of (5) (excluding one initiated at the origin) are attracted by the unit circle.

8 References

- [1] 6G Flagship. 2019. Key Drivers and Research Challenges for 6G Ubiquitous Wireless Intelligence. (2019).
- [2] Faisal Tariq, Muhammad RA Khandaker, Kai-Kit Wong, Muhammad A Imran, Mehdi Bennis, and Merouane Debbah. 2020. A speculative study on 6G. *IEEE Wireless Communications* 27, 4 (2020), 118–125.
- [3] S. Dimitrov, H.Haas, "Principles of LED Light Communications: Towards Networked Li-Fi", Cambridge University Press, 2015
- [4] R. Gagliardi, "The effect of timing errors in optical digital systems," *IEEE Trans. Commun.* vol. COM-20, no. 2, pp. 87–93, Apr. 1972.
- [5] C. Chen and C. Gardner, "Performance of PLL synchronized optical PPM communication systems," *IEEE Trans. Commun.* vol. 34, no. 10, pp. 988–994, Oct. 1986.
- [6] S. Arnon, "Visible Light Communication," Chapter 7, pp. 116-130 Cambridge University Press 2015.
- [7] S. Arnon, "The Effect of Clock Jitter in Visible Light Communication Applications," *Journal of Lightwave Technology*, Vol. 30, No. 21, November 1, 2012.

- [8] C. Danakis, M. Afgani, G. Povey, I. Underwood and H. Haas, "Using a CMOS Camera Sensor for Visible Light Communication", 3rd IEEE Workshop on Optical Wireless Communications (OWC'12), Anaheim, USA, 2012.
- [9] P. Luo, Z. Ghassemlooy, H.L. Minh, X. Tang, H. Tsai, "Undersampled Phase Shift ON-OFF Keying for Camera Communication", Sixth International Conference on Wireless Communications and Signal Processing (WCSP), 2014.
- [10] A. Costanzo, V. Loscri and M. Biagi, "Adaptive modulation control for visible light communication systems", *Journal of Lightwave Technology* 39 (9), 2780-2789, 2021.
- [11] K. O. Akande and W. O. Popoola, "Synchronization of Carrierless Amplitude and Phase Modulation in Visible Light Communication", The 3rd Workshop on Optical Wireless Communications, ICC, 2017.
- [12] David Angeli and Denis Efimov. Characterizations of input-to-state stability for systems with multiple invariant sets. *IEEE Transactions on Automatic Control*, 60(12):3242–3256, 2015.
- [13] Denis Efimov, Pierre Sacré, and Rodolphe Sepulchre. Controlling the phase of an oscillator: A phase response curve approach. In *Proceedings of the 48th IEEE Conference on Decision and Control (CDC) held jointly with 2009 28th Chinese Control Conference*, pages 7692–7697, 2009.
- [14] F.A. Delgado Rajó, V. Guerra, J.A. Rabadán Borges, J. Rufo Torres, and R. Pérez-Jiménez, "Color Shift Keying Communication System With a Modified PPM Synchronization Scheme", *IEEE Photonics Technology Letters*, Vol. 26, No. 18, September 15, 2014.
- [15] , Huai Kuei Wu and Tzu-Hung Lin, "Development of a Time Synchronization System Based on Visible Light Communication", *IEEE 4th Global Conference on Consumer Electronics (GCCE)*, 2015.
- [16] , N. Le, T. Le, T. Nguyen, and Y. Min Jang, "Synchronization Issue for Optical Camera Communications", *Seventh International Conference on Ubiquitous and Future Networks*, Sapporo, Japan, 2015.
- [17] , A. Costanzo, V. Loscri, "A Learning Approach for Robust Carrier Recovery in Heavily Noisy Visible Light Communication", *IEEE Wireless Communications and Networking Conference (WCNC)*, Marrakesh, Morocco, 2019.
- [18] M. Wolf, S. A. Cheema, and M. Haardt, "Synchronization and channel estimation for optical block-transmission systems with IM/DD", *Icton* 2016.
- [19] P. Canyelles-Pericas, A. Burton, Hoa Le-Minh, Z. Ghassemlooy, K. Busawon, "Chaos synchronization on Visible Light Communication with application for secure data communications", *IEEE Africon Conference*, Mauritius Island, 2013.
- [20] P. Canyelles-Pericas, P.A. Haigh, Z. Ghassemlooy, A. Burton, X. Dai, T. Son, H. Le-Minh, R. Binns and K. Busawon, "Chaos Synchronization in Visible Light Communications with Variable Delays Induced by Multipath Fading", *Applied System Innovation*, Vol.1, DOI 10.3390/asi1040045, 2018.
- [21] T. Liao, C.Y. Chen, H.C. Chen, Y. Y. Chen, I and Y.Y. Hou, "Realization of a Secure Visible Light Communication System via Chaos Synchronization", *Mathematical Problems in Engineering*, Special issue in Chaotic Oscillators: Theory, Experiments, Control, and Applications, Hindawi, Article ID 6661550, 2021
- [22] T. Ito, J. Tahara, M. Koike, F. Zhang, "Development of the visible light communication device for swarm using nonlinear synchronization", *Artificial Life Robotics*, DOI 10.1007/s10015-017-0396-8, 2017.
- [23] Z. Du, X. Zhou, K. Long, "A Novel Timing Synchronization Method for U-OFDM-Based Visible Light Communication", *24th Wireless and Optical Communication Conference (WOCC)*, 2014.
- [24] V. Kishore, V. Siva Prasad, V. Mani, "A Blind Timing Synchronization Algorithm for DCO-OFDM VLC Systems", *IEEE Photonics Technology Letters*, VOL. 32, NO. 17, September 1, 2020
- [25] "Time Synchronization/Stamping Method with Visible Light Communication and Energy Harvesting Method for Wireless Sensor Network inside Ariane 5 Vehicle Equipment Bay", *Data System in Aerospace Conference (DASIA)*, 2016.
- [26] X. Guo, M. Mohammad, S. Saha, Mun Choon Chan, Seth Gilbert, Derek Leong, "2PSync: Visible Light-Based Time Synchronization for Internet of Things (IoT)", *IEEE INFOCOM* 2016.
- [27] A.A. Andronov, E.A. Leontovich, I.I. Gordon, and A.G. Maier, *Theory of Bifurcations of Dynamical Systems on a Plane*. Israel Program Sci. Transl., 1971.
- [28] Yuri A. Kuznetsov, *Andronov-Hopf bifurcation*. *Scholarpedia*, 1(10):1858, 2006.
- [29] A. Costanzo and V. Loscri, "A Learning Approach for Robust Carrier Recovery in Heavily Noisy Visible Light Communication", *2019 IEEE Wireless Communications and Networking Conference (WCNC)*, Marrakesh, Morocco, 2019, pp. 1-6.
- [30] Guan-Chyun Hsieh and J. C. Hung, "Phase-locked loop techniques. A survey," in *IEEE Transactions on Industrial Electronics*, vol. 43, no. 6, pp. 609-615, Dec. 1996, doi: 10.1109/41.544547.
- [31] K. Lata and M. Kumar, "ALL Digital Phase-Locked Loop (ADPLL): A Survey", *International Journal of Future Computer and Communication*, Vol. 2, No. 6, December 2013
- [32] Huang, Shaohui, "PLL FM Demodulator with Synchronous Filter" (2012). *Theses and Dissertations*. Paper 1285
- [33] D. Efimov, P. Sacré and R. Sepulchre, "Controlling the phase of an oscillator: A phase response curve approach," *Proceedings of the 48th IEEE Conference on Decision and Control (CDC) held jointly with 2009 28th Chinese Control Conference*, 2009, pp. 7692-7697.
- [34] Efimov, D.V. Phase resetting control based on direct phase response curve. *J. Math. Biol.* 63, 2011, 855–879.
- [35] Chen, Z, Basnayaka, D, Wu, X and Haas, H., "Interference Mitigation for Indoor Optical Atto-cell Networks using Angle Diversity Receiver", *Journal of Lightwave Technology*, vol. 36, no. 18, 2018. <https://doi.org/10.1109/JLT.2018.2848221>
- [36] A. Costanzo, V. Loscri, V. Deniau, J. Rioult, "On the Interference Immunity of Visible Light Communication (VLC)", *Globecom* 2020.
- [37] E. Panteley, A. Loría and A. El Ati, "Analysis and control of Andronov-Hopf oscillators with applications to neuronal populations," *2015 54th IEEE Conference on Decision and Control (CDC)*, 2015, pp. 596-601.
- [38] M. Rahaim and T. D. C. Little, "Optical interference analysis in Visible Light Communication networks," *2015 IEEE International Conference on Communication Workshop (ICCW)*, London, 2015, pp. 1410-1415.
- [39] K. Lata and M. Kumar, "ALL Digital Phase-Locked Loop (ADPLL): A Survey", *International Journal of Future Computer and Communication*, Vol. 2, No. 6, December 2013
- [40] Huang, Shaohui, "PLL FM Demodulator with Synchronous Filter", *Theses and Dissertations*, Lehigh University, Paper 1285, 2012.